J. Electrochem. Sci. Eng. **10(4)** (2020) 335-346; http://dx.doi.org/10.5599/jese.861

Open Access: ISSN 1847-9286

www.jESE-online.org

Original scientific paper

BSA-binding studies of 2- and 4-ferrocenylbenzonitrile: voltammetric, spectroscopic and molecular docking investigations

Hacen Benamara, Touhami Lanez✉ and Elhafnaoui Lanez

University of El Oued, Chemistry Department, VTRS Laboratory, B.P.789, 39000, El Oued, Algeria

Corresponding author: ✉lanezt@gmail.com; Tel.: +213-661655550

Received: May 29, 2020; Revised: June 11, 2020; Accepted: June 15, 2020

Abstract

The binding affinity of 2-ferrocenylbenzonitrile (2FBN) and 4-ferrocenylbenzonitrile (4FBN) with bovine serum albumin (BSA) has been investigated by cyclic voltammetry, absorption spectroscopy and molecular modelling techniques. The results indicated that both of the two derivatives could bind to BSA and cause conformational changes with the order 2FBN > 4FBN. The voltammetric behavior of 2FBN and 4FBN before and after the addition of BSA suggests that the electrochemical reaction is kinetically controlled by the diffusion step and demonstrated that diffusion coefficients of 2FBN-BSA and 4-FBN-BSA complexes are lower than that of free compounds. Molecular docking suggested that the binding mode of the two compounds to BSA is of hydrophobic and hydrogen bond interactions, moreover the ligand 2FBN additionally show a π-cation interaction.

Keywords

Cyclic voltammetry; ferrocene derivatives; binding constant; interactions; modelling; in silico; in vitro

Introduction

Nitriles and cyanides are compounds containing a -CN functional group in their molecular structure. In nitriles the -CN functional group is attached to an organic structure [1], but in cyanides, it is attached to an inorganic compound [2]. Cyanides are toxic because they denote the highly toxic inorganic salts of hydrogen cyanide, while nitriles are not toxic because they do not release cyanide ions [3,4]. The non-toxic properties of nitriles encouraged researchers to study their pharmaco-chemistry as potential drugs. The prevalence of nitrile-containing drugs shows the biocompatibility of the nitrile functionality [5,6]. Recently many pharmaceuticals drugs containing nitriles are either prescribed for many different types of diseases or are in clinical trial [6].

Nitrile groups are usually known as hydrogen bond acceptors [7-9], many studies show the formation of hydrogen bonding between the nitrogen atom of the nitrile group and amino acids of

protein backbone [10-13]. The bonds are often established between the nitrile and the expected hydrogen bond of the donor serine or arginine amino acids.

Serum albumin is the most important protein in blood plasma and plays a vital role in the transport and distribution of metals, fatty acids, hormones, and renders toxins harmless by transporting them to disposal sites. In addition, BSA binds to variety drugs at multiple sites in the body vascular system [14-16].

BSA interactions with small molecules have become increasingly important in pharmacochemistry and are commonly used as key steps in the construction of medicinal compounds [17-21]. The research in this field provides strong support for BSA-binding studies and a deeper understanding of the way medicaments target and bind receptors [22,23]. BSA interactions with small molecules also help in understanding the toxicity, pharmacokinetics, biochemistry, pharmacodynamics, and distribution of molecules in the organism. Thus, the investigation of BSA interactions with small molecules has been an important analysis in medicinal chemistry and clinical medicine [24].

The pharmacochemistry of ferrocene derivatives has attracted the attention of many scientists, and their study has been encouraged by potential biological applications [25-27]. Many ferrocene derivatives that have been studied in the last decade show important biological activities, such as cytotoxic [28-30], antimicrobial [31,32] and antitumor [33-38] activities.

The incorporation of the ferrocenyl moiety into the structure of biologically active molecules may lead to the increase of their biological activities, based on the fact that nitriles-containing ferrocenes are expected to be more pharmacologically active than free nitriles. In this context the present study surveys the interaction of two nitrile-containing ferrocene with BSA by focusing on the roles of the -CN functional groups. The study was carried out in 0.1 M 90 % DMF/buffer phosphate solution at pH 7.4 using voltammetric, spectroscopic and molecular docking techniques.

Experimental

Synthesis

2-ferrocenylbenzonitrile (2FBN) and 4-ferrocenylbenzonitrile (4FBN) addressed in this work are shown in Figure 1a and 1b, and were synthesised by the coupling reaction between ferrocene and the diazonium salts of the corresponding cyanoaniline, as reported previously by our group [39]. The crystal structure of BSA was taken from protein databank (https://www.rcsb.org/, PDB ID: 4f5s) (Figure 1c).

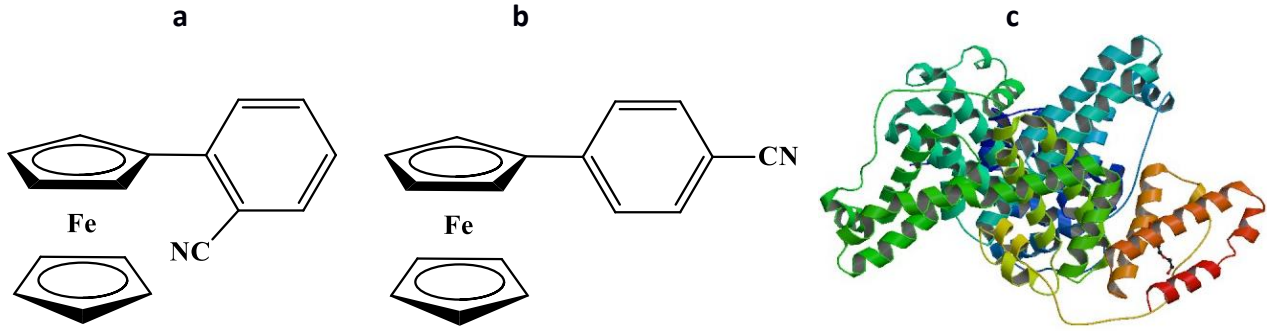

Figure 1. *Chemical structures of (a) 2-ferrocenylbenzonitrile, (b) 4-ferrocenylbenzonitrile and (c) structure of BSA (ID: 4f5s)*

Chemicals

All reagents and solvents were of analytical grade and obtained from commercial sources and used without further purification. BSA was obtained from Merck and used as received, while its

concentration was determined by the extinction coefficient of 44300 M^{-1} cm^{-1} at 280 nm [40]. All stock solutions were used within 5 days after preparation and stored at 4 °C until use. The phosphate buffer solution was prepared using sodium dihydrogen phosphate and disodium hydrogen phosphate (Sigma Aldrich) and double-distilled water. The physiological pH (pH 7.4) was maintained by this phosphate buffer. N,N-Dimethylformamide (DMF) (HPLC-grade; Sigma-Aldrich) was used as the solvent in voltammetric and spectroscopic assays. Tetrabutylammonium tetra-fluoroborate (Bu_4NBF_4) (electrochemical grade 99 %; Sigma-Aldrich) was used as the supporting electrolyte. Nitrogen gas was provided from a cylinder (research grade (99.99 %); Linde gaz Algérie).

Materials and measurements

Voltammetric assays were performed using a PGZ301 voltammeter running on VoltaMaster 4 V 7.08 software (Radiometer Analytical SAS, France). The concentration of the supporting electrolyte was kept at 0.1 M all time. The air was removed from the solution by bubbling nitrogen gas through it. Experiments were run in a three-electrode electrochemical cell containing a glassy carbon (GC) working electrode with a geometric area of 0.013 cm^2, a platinum wire as counter (auxiliary) electrode and Hg/Hg_2Cl_2 paste covered wire as reference electrode.

Absorption spectra measurements were conducted on a UV-Vis spectrometer, (Shimadzu 1800, Japan), using the cell of length 1 cm.

Chemical structures of 2FBN and 4FBN were optimized by Gaussian 09 program package [41], using density functional theory (DFT) and the B3LYP level of theory [42,43] with 6-311++G(d,p) basis set.

The molecular docking studies were done using AutoDock 4.2 docking software [44,45], all docking studies were executed on a Pentium 2.20 GHz and RAM 4.00 Go microcomputer MB memory with windows 10 operating system.

Results and discussion

Cyclic voltammetric study

BSA-2FBN and BSA-4FBN complexes in 0.1 M 90 % DMF/buffer phosphate solution at pH 7.4 were used. Various concentrations of BSA were added into 12 ml solution of 100 µM of the ligand solutions, and the voltammograms were recorded in the potential range of 0.1 to 0.8 V *vs.* Hg/Hg_2Cl_2 at 28 ± 1 °C.

Many studies on the interaction of BSA with small molecules in this potential range have been carried out using cyclic voltammetry techniques, and all these studies have shown that BSA does not show any adsorption on the bare electrode surface at this potential range [46-50]. Adsorption of BSA can only appear at negative potential [51].

The cyclic voltammograms (Figure 2) of 2FBN and 4FBN at different concentrations of BSA show respectively oxidation and reduction maximums in a reversible electrochemical process. Addition of an increasing amount of BSA solution results in a decrease in peak current height with a positive shift in peak potential position. This decrease in anodic peak current height is exploited for the calculation of the binding parameters.

The binding constant, K_b, was calculated from the observed cyclic voltammetry data, using the following equation [52]:

$$\log\frac{1}{c_{BSA}} = \log K_b + \log\frac{i}{i_0 - i} \quad (1)$$

where C_{BSA} is BSA concentration, K_b represents the binding constant, while i_0 and i indicate the anodic peak current density of the free and BSA-bound compounds, respectively.

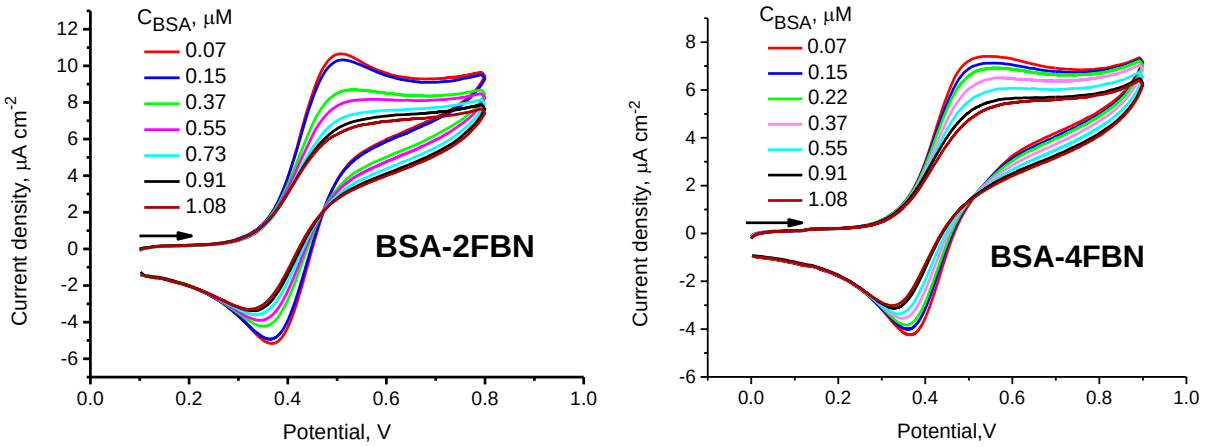

Figure 2. *Cyclic voltammograms of BSA–2FBN and BSA–4FBN complexes at different concentration of BSA. 2FBN and 4FBN concentrations were kept at 100 µM*

Obviously, K_b can be determined from the intercept of the plot of log $(1/C_{BSA})$ *vs.* log $(i/(i_0-i))$. These plots are for 2FBN and 4FBN represented in Figure 3, from which the values of binding constants were determined as 7.05×10^5 M^{-1} for 2FBN and 3.44×10^5 M^{-1} for 4FBN. The binding free energy changes calculated using the equation $\Delta G = -nRT \ln K_b$ are found equal to -33.94 and -32.14 kJ mol^{-1}, respectively. The order of magnitude and the sign of the obtained binding free energy indicate respectively the electrostatic mode and the spontaneity of interactions between the compounds and BSA.

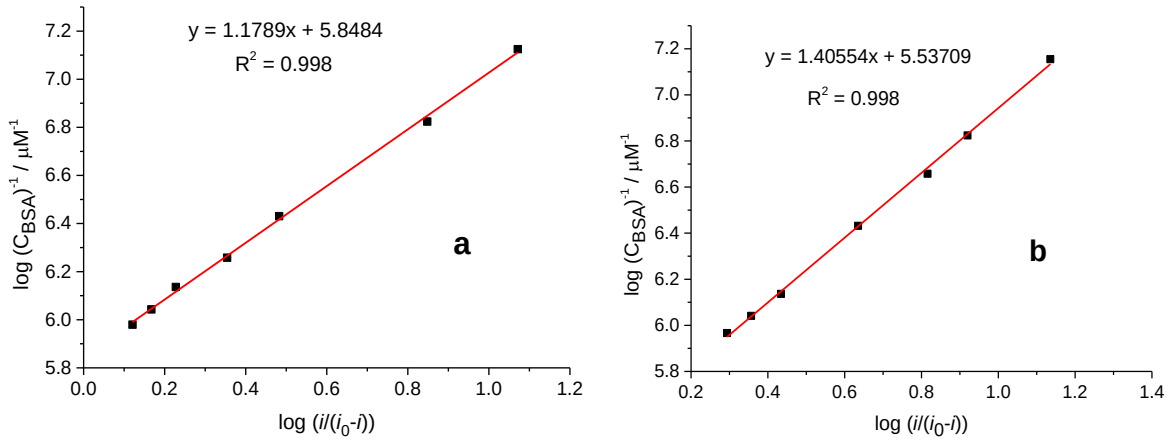

Figure 3. *Plots of log $(C_{BSA})^{-1}$ vs. log $(i/(i_0-i))$ used to calculate BSA binding constants: (a) 2FBN, (b) 4FBN*

Ratio of binding constants

The ratio of the binding constants of the reaction of the reduced form FBN (FBN represents 2FBN or 4FBN) with BSA to that of the oxidized form $[FBN]^+$, could be calculated from the voltammograms of Figure 4, which represent the cyclic voltammograms of 100 µM solution of 2FBN and 4FBN in the absence and presence of 0.37 µM of BSA. The shift in the anodic and cathodic peak potential values caused by the addition of BSA can be used to calculate the ratio of binding constants [53].

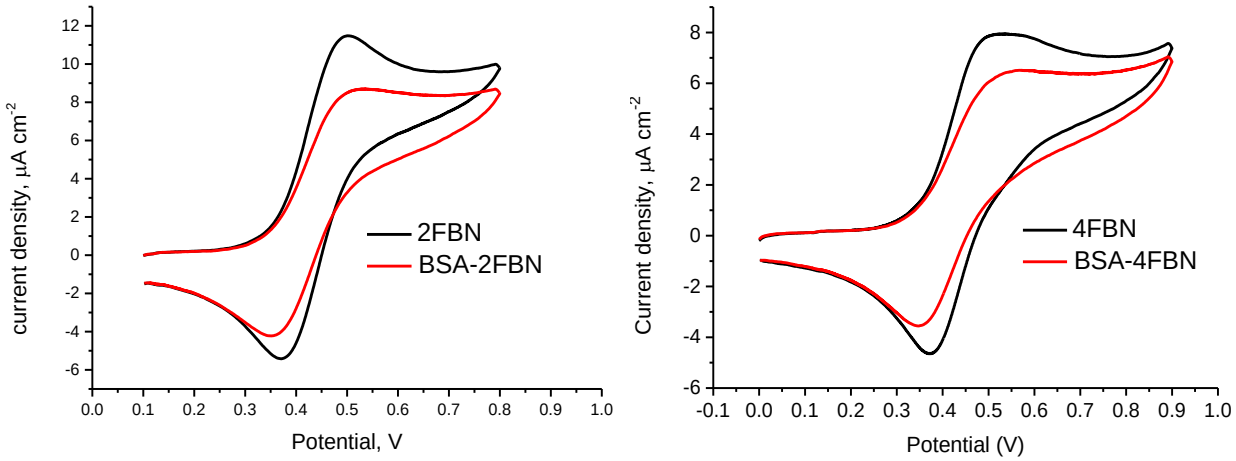

Figure 4. *Cyclic voltammograms of the free compounds (100 µM) and their BSA complexes (0.37 µM), scan rate 100 mV s^{-1}*

In such case when both the anodic and cathodic peak potential values are shifted upon the addition of BSA, the following equilibriums can be applied [54]:

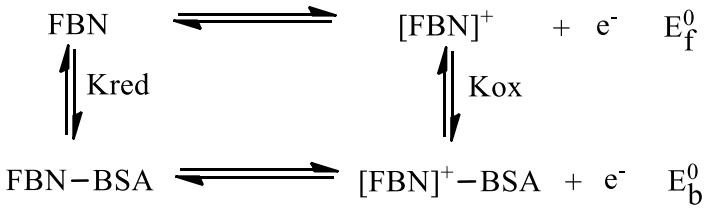

Figure 5. *Redox process of studied compounds with BSA, FBN represents 2FBN or 4FBN.*

The application of the Nernst relation to the equilibriums of Figure 5 produces the following equation:

$$\Delta E^0 = E_b{}^0 - E_f{}^0 = E^0(\text{FBN-BSA}) - E^0(\text{FBN}) = 0.06 \log \frac{K_{red}}{K_{ox}} \quad (2)$$

In equation (2), $E_f{}^0$ and $E_b{}^0$ are the formal potentials of the FBN^+/FBN couple of free and BSA-bound compounds, respectively. The formal potential shift ΔE^0 calculated on the basis of the voltammograms of Figure 4, are summarized in Table 1. The ratios of the binding constants were calculated from equation (2) by replacing ΔE^0 taken from Table 1.

Table 1. *Electrochemical data of free and BSA-bound 2FBN and 4FBN used to calculate the ratio of the binding constants.*

Sample code	E_{pa} / V	E_{pc} / V	E^0 / V	ΔE^0/ mV	K_{red} / K_{ox}
2FBN	0.502	0.369	0.4355	3.5	1.14
2FBN-BSA	0.527	0.351	0.439		
4FBN	0.538	0.374	0.456	4.0	1.16
4FBN-BSA	0.572	0.348	0.46		

The obtained ratios of the binding constants indicate that the reduced form of both 2FBN and 4FBN bind slightly stronger to BSA than their oxidized forms.

Diffusion coefficients

The diffusion coefficients of the free and BSA-bound 2FBN and 4FBN compounds were obtained from their electrochemical behavior represented in Figures 6 and 7. These cyclic voltammograms were obtained by varying the potential scan rates of 100 µM of the free compounds in the absence

and presence of 0.91 µM of BSA. All the voltammograms present well-defined stable redox peaks attributed to the redox process of 2FBN and 4FBN.

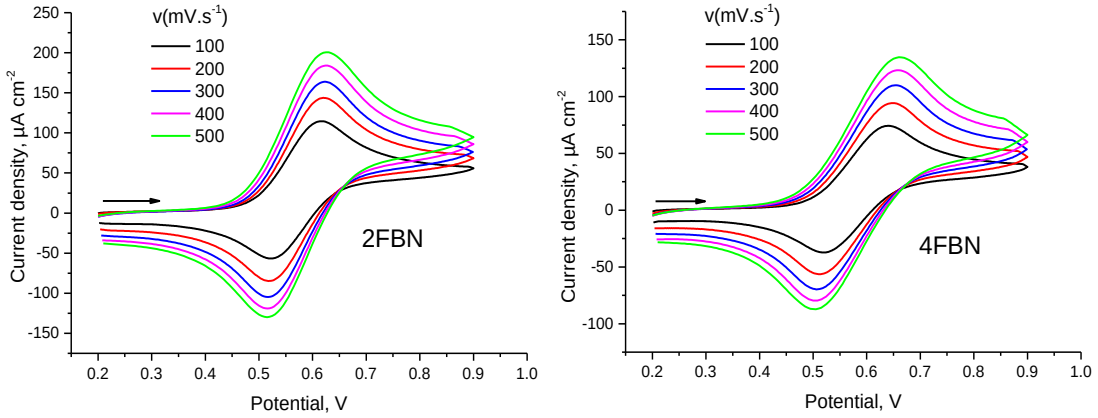

Figure 6. *Cyclic voltammetric behavior of 100 µM of 2FBN and 4FBN in 0.1 M 90 % DMF/buffer phosphate solution at different scan rates.*

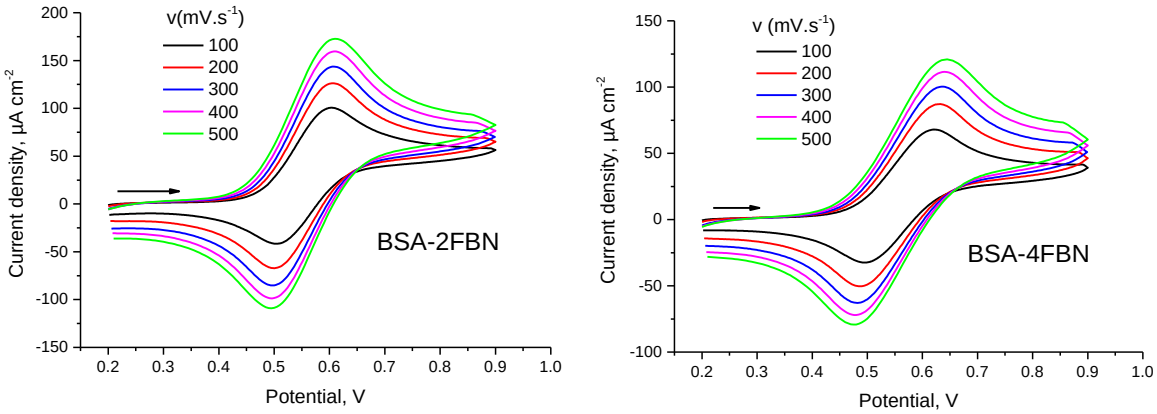

Figure 7. *Cyclic voltammetric behavior of 0.91 µM of BSA-2FBN and BSA-4FBN in 0.1 M 90 % DMF/buffer phosphate solution at different scan rates*

Diffusion coefficients of FBN-BSA in the solution with an excess of BSA were calculated from the voltammograms of Figures 6 and 7 using the following Randles–Ševčik equation [55]:

$$i_{pa} = 2.69 \times 10^5 n^{\frac{3}{2}} S C D^{\frac{1}{2}} v^{\frac{1}{2}} \quad (3)$$

In equation (3), i_{pa} represents the anodic peak current (A), n is the number of electrons participated in the oxidation process, S is the surface of the working electrode (cm^2), C is the concentration of the electroactive compounds (mol cm^{-3}), D is the diffusion coefficient ($cm^2\ s^{-1}$), and v is the scan rate (V s^{-1}). The plots of i_{pa} *vs*. $v^{1/2}$ in Figure 8 suggest that the oxidation reaction is diffusion controlled. The diffusion coefficients of the free and BSA-bound compounds were calculated from the slopes of linear regressions of the plots of i_{pa} *vs*. $v^{1/2}$. The lower diffusion coefficients of the bound compounds as compared to the free once, further confirm the interaction between the studied compounds and BSA (Table 2).

Table 2. *Diffusion constant values of the free and BSA bound form of 2FBN and 4FBN.*

Sample code	Equation	R^2	$D \times 10^6$/ $cm^2\ s^{-1}$
2FBN	y = 6.94x + 44.25	0.999	3.94
2FBN-BSA	y = 5.78x + 42.97	0.999	2.73
4FBN	y = 4.89x + 24.63	0.999	1.96
4FBN-BSA	y = 4.22x + 26.40	0.999	1.46

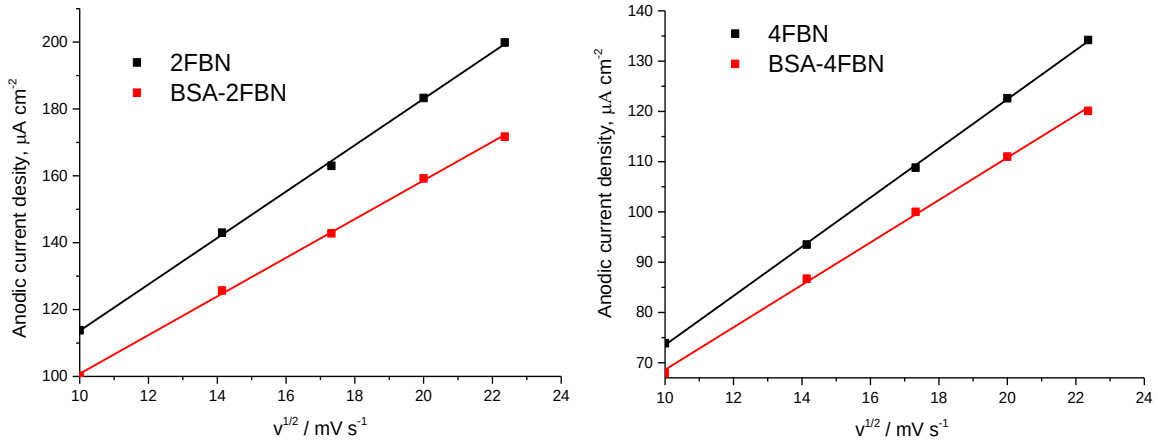

Figure 8. *i_{pa} vs. $v^{1/2}$ plots of 100 µM 2FBN and 4FBN in the absence and in presence of 0.91 µM BSA based on voltammograms in Figures 6 and 7.*

Absorption spectroscopic studies

The interactions of 2FBN and 4FBN with BSA were also studied by absorption spectroscopic titration. The purpose of this study was to validate the results obtained from cyclic voltammetry assays. The experiments were carried out with 0.1 M 90 % DMF/buffer phosphate solution of pH 7.4. Incremental portions of BSA solution from 0.34 to 0.70 µM for 2FBN and from 0.15 to 2.67 µM for 4FBN were added to the same solution containing 0.5 mM of 2FBN and 2 mM of 4FBN. The obtained mixture was scanned in the range of 300–600 nm. BSA does not show any absorption at this wavelength, while the strong peak which appeared at 434.5 nm (due to π→π* transition in the conjugated ring of ferrocene moiety) lowered in intensity upon continuous addition of BSA to 2FBN and 4FBN (Figure 9).

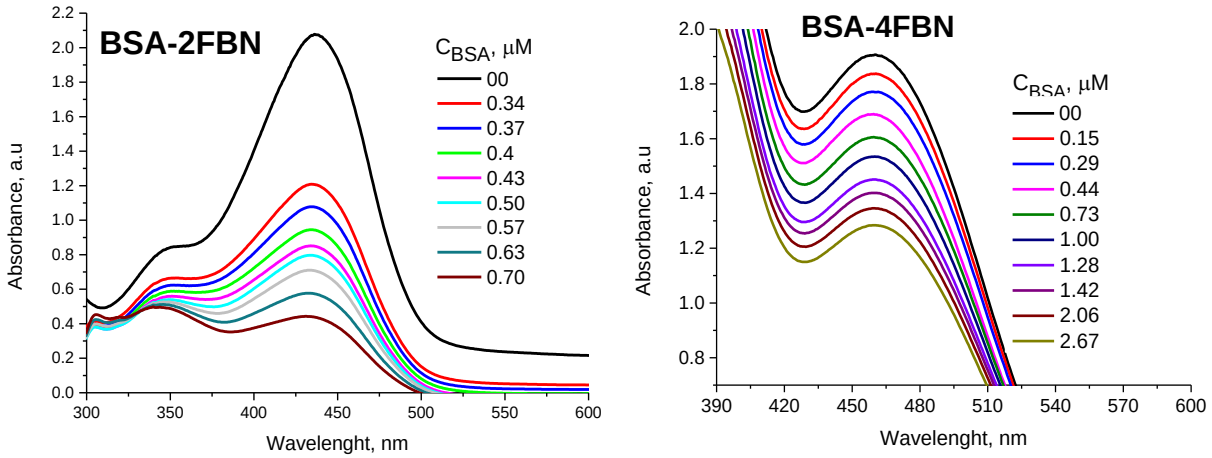

Figure 9. *Absorbance spectra of 2FBN-BSA and 4FBN-BSA complexes. 2FBN and 4FBN concentrations were kept respectively at 0.5 and 2 mM*

The binding constant K_b was evaluated from the absorption data according to Benesi-Hildebrand equation [56]:

$$\frac{A_0}{A-A_0} = \frac{\varepsilon_f}{\varepsilon_b-\varepsilon_f} + \frac{\varepsilon_f}{\varepsilon_b-\varepsilon_f}\frac{1}{K_b C_{BSA}} \quad (4)$$

In equation (4), A_0 and A are absorbencies of the ligands and their complexes with BSA, respectively, while ε_f and ε_b are their extinction coefficients. The plot of $A_0/(A_0\text{-}A)$ *vs.* $1/C_{BSA}$ gave a

slope of $\varepsilon_f/(\varepsilon_b - \varepsilon_f)K_b$, and intercept equal to $\varepsilon_f/(\varepsilon_b - \varepsilon_f)$, where K_b is the ratio of the slope to the intercept (Figure 10). The value of K_b has been determined to be 7.18×10^5 for 2FBN-BSA and 2.79×10^5 M^{-1} for 4FBN-BSA. The corresponding free binding energies calculated using the equation $\Delta G = -nRT \ln K_b$ were equal to -33.77 and -31.40 kJ mol^{-1}, respectively. These values are in good agreement with those obtained from cyclic voltammetry experiments.

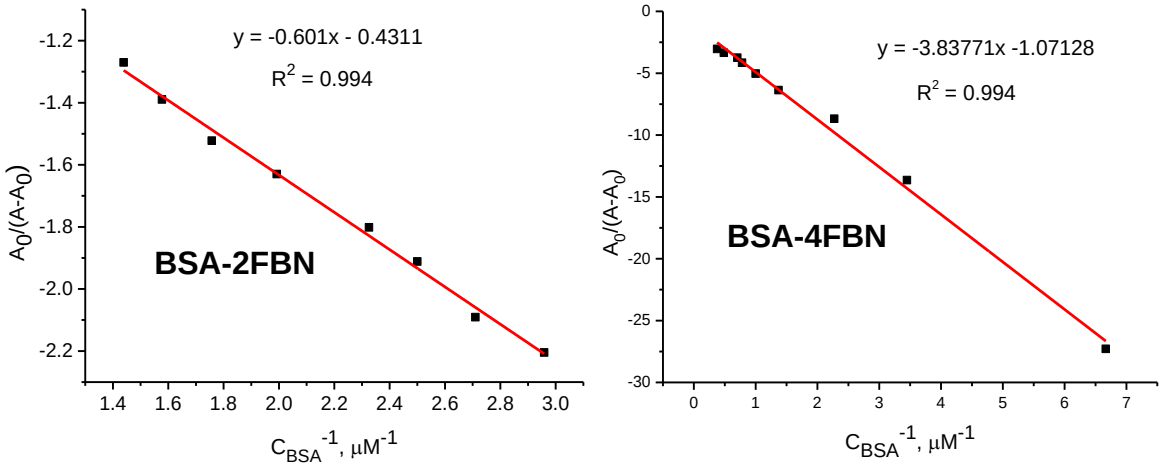

Figure 10. *Plots of $A_0/(A_0-A)$ vs. C_{BSA}^{-1} used to calculate the binding constants of BSA-2FBN and BSA-4FBN*

Docking setup

Geometry optimization

Density functional theory (DFT) was used for the optimisation without imposing any symmetry constraints and calculations were realized with the Gaussian 09 package. The exchange functional of Becke, and the correlation functional of Lee, Yang and Parr (B3LYP) were employed with 6-311++G(d,p) basis set. The optimized structures of the compounds are depicted in Figure 11.

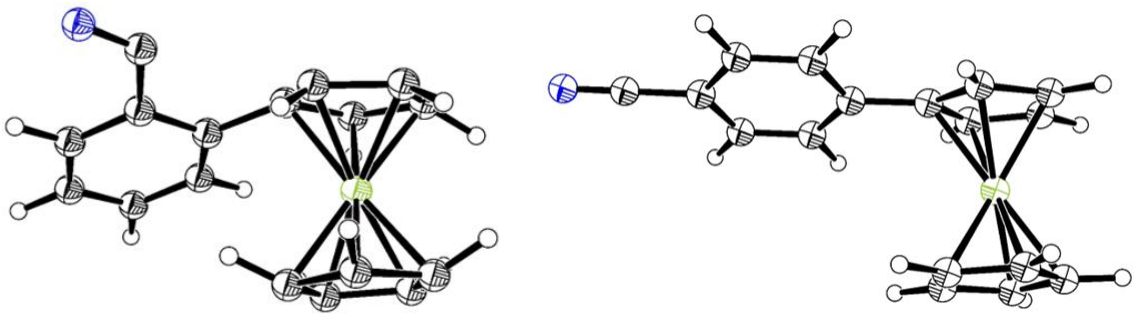

Figure 11. *The optimized structures of 2FBN and 4FBN (ORTEP View 03, V1.08); color codes are carbon (grey), hydrogen (white), nitrogen (blue), iron (green).*

Molecular docking studies

In order to confirm and interpret the results of cyclic voltammetric and spectrophotometric measurements and recognize the way in which 2FBN and 4FBN bind to BSA, semi flexible docking was carried out using AutoDock 4.2 along with the AutoDock Vina software. The crystal structure of BSA was taken from the protein databank (https://www.rcsb.org/, PDB ID: 4f5s). The PDB file was imported into AutoDock Tools, all hydrogen atoms and gassier charges were added. During all docking process, BSA kept rigid while all the bonds of the ligands were set free. The grid map with 0.375 Å spacing and 126×70×100 points were generated. The docking experiment comprised of 100 docking

runs with 150 individuals and 2.500.000 energy evaluations. Lamarckian genetic algorithm was used in the docking, and other parameters were set as default. The stable conformation which corresponds to the lowest binding energy was used for docking analysis. The visualization of the interaction was generated with PLIP web service (protein Ligand Interaction Profiler).

Results from molecular docking suggest that hydrogen bonding, hydrophobic forces and π-cation interaction are involved in the binding process. Figure 12 illustrates the interaction of 2FBN and 4FBN with the nearby residues in the active site of BSA.

The interacting residues, distances, and type of interactions are summarised in Tables 3 and 4.

Table 3. *Hydrophobic interactions between the ligands 2FBN and 4FBN with BSA.*

Interaction type	Residue	Amino acid	Distance, Å
BSA-BSA	80A	LEU	2.85
	81A	ARG	3.45
	88A	ALA	3.72
BSA-4FBN	115B	LEU	3.99
	115B	LEU	3.57
	122B	LEU	3.14
	136B	LYS	3.94
	137B	TYR	3.15
	140B	GLU	3.68
	141B	ILE	3.58
	160B	TYR	3.96

Table 4. *Hydrogen bonds between the ligands 2FBN and 4FBN and BSA.*

Interaction type	Residue	Amino acid	Distance H-A, Å	Distance D-A, Å
2FBN-BSA	81A	ARG	3.00	3.45
	82A	GLU	2.04	3.05
	82A	GLU	3.22	3.71
4FBN-BSA	137B	TYR	2.38	3.32

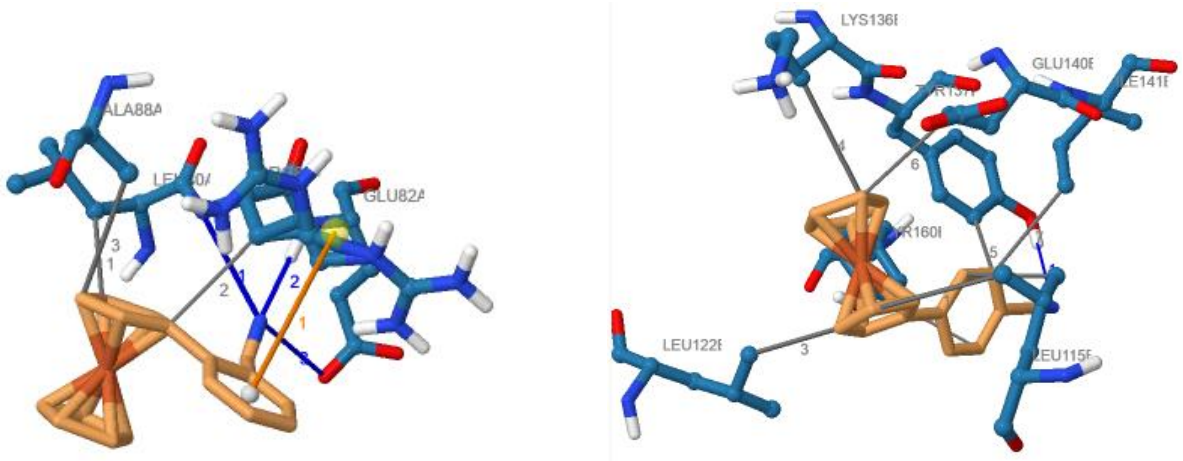

BSA-2FBN BSA-4FBN

Figure 12. *Best docking poses for BSA-2FBN and BSA-4FBN generated with PLIP web service illustrating the hydrophobic and H-bons interactions. Elements colors: hydrogen, oxygen, nitrogen, and iron are represented in white, red, blue and brown, respectively Color code: Hydrogen bonds: bleu lines, hydrophobic interactions: gray lines, π-Cation interactions: beige lines.*

The compound 2FBN formed three hydrogen bonds between amino acid residues Arg-81 and Glu-82 as donors and the polar groups of the ligand – nitrile group. 4FBN formed only one hydrogen bond between the residue Tyr-137 as acceptor and the nitrogen of the 4FBN as a donor, table 4. The distances in table 4 are between hydrogen and the receptor atoms (H-A), and between donor and receptor atoms (D-A). Furthermore, for the complex 2FBN-BSA, molecular docking results also suggested a π-cation interaction between the positively charged amino acid residue Arg-81 and the benzene ring within a distance of 5.01 Å.

The ligand 4FBN interacted through hydrophobic interactions with the residues Leu-115, Leu-122, Lys-136, Tyr-137, Glu-140, Ile-141, and Tyr-160,

The binding free energy of the docked structure of 2FBN and 4FBN ligands with BSA was found to be -32.89 and -31.26 kJ mol^{-1}, respectively. The binding constant K_b calculated using the equation $\Delta G = -nRT \ln K_b$ was found to be 5.77×10^5 and 2.99×10^5 mol^{-1}, respectively. These results are supported by the absorption spectroscopy and cyclic voltammetry experiments. Overall, molecular docking results are in good agreement with the data obtained from experimental assays.

Conclusions

In the present work, we applied experimental and theoretical methods for the determination of binding proprieties of two nitrile-containing ferrocenes with BSA. Binding free energies for the interaction of 2FBN and 4FBN with BSA, obtained from voltammetric experiments, were respectively -33.95 and -32.14 kJ mol^{-1}, and these values are in good agreement with those obtained from adsorption spectroscopic assays (-33.77 and -31.40 kJ mol^{-1}). The low diffusion coefficient values of the BSA-bound 2FBN and 4FBN as compared to the corresponding free 2FBN and 4FBN, further confirm the formation of the complexes 2FBN-BSA and 4FBN-BSA which diffuses more slowly compared to the free compounds due to their higher molecular weight. Molecular docking study further confirms the obtained experimental results and allows the visualisation of interactions and determination of bonds length formed between the ligands and the amino acid residues of BSA.

***Acknowledgements**: The authors are grateful to the Algerian Ministry of Higher Education and Research for financial support (project code: B00L01UN390120150001).*

References

[1] *Compendium of Polymer Terminology and Nomenclature, IUPAC Recommendations 2008,* R. G. Jones, J. Kahovec, R. Stepto, E. S. Wilks, M. Hess, T. Kitayama, W. Val Matanomski (Eds.). With advice from A. Jenkins and P. Kratochvil, The Royal Society of Chemistry, Cambridge, UK, 2009, p. 98.

[2] *Nitriles - MeSH - NCBI*, (n.d.). https://www.ncbi.nlm.nih.gov/mesh/68009570 (accessed April 22, 2020).

[3] J. Wit, H. Van Genderen, *Biochemical Journal* **101(3)** (1966) 698-706.

[4] D. H. Hutson, E. C. Hoadley, M. H. Griffiths, C. Donninger*, Journal of Agricultural and Food Chemistry* **18(3)** (1970) 507-512.

[5] S. T. Murphy, H. L. Case, E. Ellsworth, S. Hagen, M. Huband, T. Joannides, C. Limberakis, K. R. Marotti, A. M. Ottolini, M. Rauckhorst, J. Starr, M. Stier, C. Taylor, T. Zhu, A. Blaser, W. A. Denny, G. L. Lu, J. B. Smaill, F. Rivault, *Bioorganic and Medicinal Chemistry Letters* **17(8)** (2007) 2150-2155.

[6] F. F. Fleming, L. Yao, P. C. Ravikumar, L. Funk, B. C. Shook, *Journal of Medicinal Chemistry* **53(22)** (2010) 7902-7917.

[7] J-Y. Le Questel, M. Berthelot, C. Laurence, *Journal of Physical Organic Chemistry* **13(6)** (2000) 347-358.

[8] C. Laurence, K. A. Brameld, J. Graton, J. Y. Le Questel, E. Renault, *Journal of Medicinal Chemistry* **52(14)** (2009) 4073-4086.

[9] A. Allerhand, P. von Rague Schleyer, *Journal of the American Chemical Society* **85(7)** (1963) 866-870.

[10] Y. Wang, Y. Du, N. Huang, *Future Medicinal Chemistry* **10(23)** (2018) 2713-2728.
[11] L. Xue, F. Zou, Y. Zhao, X. Huang, Y. Qu, *Spectrochimica Acta - Part A: Molecular and Biomolecular Spectroscopy* **97** (2012) 858-863.
[12] R. E. Royer, M. Kibirige, C. R. Tafoya, D. L. Vander Jagt, L. M. Deck, *Journal of Pharmaceutical Sciences* **77(3)** (1988) 237-240.
[13] J. T. First, J. D. Slocum, L. J. Webb, *Journal of Physical Chemistry B* **122(26)** (2018) 6733-6743.
[14] T. Peters Jr., *All about albumin: biochemistry, genetics, and medical applications*, Academic Press Inc., San Diego, California, 1996, p. 382.
[15] M. Fasano, S. Curry, E. Terreno, M. Galliano, G. Fanali, P. Narciso, S. Notari, P. Ascenzi, *IUBMB Life* **57(12)** (2005) 787-796.
[16] P. Lee, X. Wu, *Current Pharmaceutical Design* **21(14)** (2015) 1862-1865.
[17] T. Topală, A. Bodoki, L. Oprean, R. Oprean, *Clujul Medical* **87(4)** (2014) 215-219.
[18] L. Zhang, Q. Y. Cai, Z. X. Cai, Y. Fang, C. S. Zheng, L. L. Wang, S. Lin, D. X. Chen, J. Peng, *Molecules* **21(12)** (2016) 1706. https://doi.org/10.3390/molecules21121706.
[19] Q. Zhang, Y. Ni, *RSC Advances* **7(63)** (2017) 39833-39841.
[20] D. Sood, N. Kumar, G. Rathee, A. Singh, V. Tomar, R. Chandra, *Scientific Reports* **8** (2018) 16964. doi.org/10.1038/s41598-018-35384-6.
[21] J. Yu, J.-Y. Liu, W.-M. Xiong, X.-Y. Zhang, Y. Zheng, *BMC Chemistry* **13** (2019). 95. https://doi.org/-10.1186/s13065-019-0615-6.
[22] D. Sleep, *Expert Opinion on Drug Delivery* **12** (2015) 793–812.
[23] G. L. Francis, *Cytotechnology* **62(1)** (2010) 1-16.
[24] A. M. Bagoji, J. I. Gowda, N. M. Gokavi, S.T. Nandibewoor, *Journal of Biomolecular Structure and Dynamics* **35(11)** (2017) 2395-2406.
[25] F. A. Larik, A. Saeed, T. A. Fattah, U. Muqadar, P. A. Channar, *Applied Organometallic Chemistry* **31(8)** (2016), doi.org/10.1002/aoc.3664.
[26] M. Patra, G. Gasser, *Nature Reviews Chemistry* **1(9)** (2017) 0066. https://doi.org/10.1038/s41570-017-0066.
[27] M. Patra, G. Gasser, M. Wenzel, K. Merz, J. E. Bandow, N. Metzler-Nolte, *Organometallics* **29(19)** (2010) 4312-4319.
[28] M. Görmen, P. Pigeon, S. Top, E. A. Hillard, M. Huché, C. G. Hartinger, F. de Montigny, M. A. Plamont, A. Vessières, G. Jaouen, *ChemMedChem* **5** (2010) 2039-2050.
[29] W. I. Pérez, Y. Soto, C. Ortíz, J. Matta, E. Meléndez, *Bioorganic and Medicinal Chemistry* **23(3)** (2015) 471-479.
[30] J. Yong, X. Wang, X. Wu, C. Lu, *Journal of Infectious Diseases & Therapy* **5(1)** (2017) 1000311. https://doi.org/10.4172/2332-0877.1000311.
[31] A. S. Hassan, T. S. Hafez, *Journal of Applied Pharmaceutical Science* **8(5)** (2018) 156-165.
[32] S. Li, Z. Wang, Y. Wei, C. Wu, S. Gao, H. Jiang, X. Zhao, H. Yan, X. Wang, *Biomaterials* **34(4)** (2013) 902-911.
[33] H. Benamara, T. Lanez, *Journal of Fundamental and Applied Sciences* **11(3)** (2019) 1267-1278.
[34] A. Adaika, T. Lanez, E. Lanez, *Journal of Fundamental and Applied Sciences* **11(2)** (2019) 748-768.
[35] E. Lanez, L. Bechki, T. Lanez, *Chemistry and Chemical Technology* **13(1)** (2019) 11-17.
[36] X. Gao, G. Gong, Z. Zhang, G. Du, Y. Cao, G. Zhao, *Journal of Molecular Structure* **1200** (2020) 127077. https://doi.org/10.1016/j.molstruc.2019.127077
[37] S. Sansook, E. Lineham, S. Hassell-Hart, G. J. Tizzard, S. J. Coles, J. Spencer, S. J. Morley, *Molecules* **23(9)** (2018) 2126. https://doi.org/10.3390/molecules23092126.
[38] S. Realista, S. Quintal, P. N. Martinho, A. I. Melato, A. Gil, T. Esteves, M. de Deus Carvalho, L. P. Ferreira, P. D. Vaz, M. J. Calhorda, *Journal of Coordination Chemistry* **70(2)** (2017) 314-327.
[39] T. Lanez, P. L. Pauson, *Journal of the Chemical Society, Perkin Transactions* **1** (1990) 2437-2442.
[40] A. Ray, B. Koley Seth, U. Pal, S. Basu, *Spectrochimica Acta - Part A: Molecular and Biomolecular Spectroscopy* **92** (2012) 164-174.
[41] M. Frisch, G. Trucks, H. Schlegel, G. E. Scuseria…, *Gaussian 09,* Gaussian Inc., Wallingford, 2009.
[42] B. Miehlich, A. Savin, H. Stoll, H. Preuss, *Chemical Physics Letters* **157(3)** (1989) 200-206.
[43] A. D. Becke, *The Journal of Chemical Physics* **98(7)** (1993) 5648-5652.

[44] G. M. Morris, H. Ruth, W. Lindstrom, M. F. Sanner, R. K. Belew, D. S. Goodsell, A. J. Olson, *Journal of Computational Chemistry* **30(16)** (2009) 2785-2791.
[45] O. Trott, A. J. Olson, *Journal of Computational Chemistry* **31(2)** (2009) 455-461.
[46] S. Bi, L. Yan, B. Wang, J. Bian, Y. Sun, *Journal of Luminescence* **131(5)** (2011) 866-873.
[47] M. Mahanthappa, B. G. Gowda, J. I. Gowda, R. Rengaswamy, *Journal of Electrochemical Science and Engineering* **6(2)** (2016) 155-164.
[48] J. B. M. Leuna, S. K. Sop, S. Makota, E. Njanja, T. C. Ebelle, A. G. Azebaze, E. Ngameni, A. Nassi, *Bioelectrochemistry* **119** (2018) 20–25.
[49] S. Pramanik, R. Chakraborty, *International Journal of Biosensors & Bioelectronics* **2(3)** (2017) 96-98.
[50] J. Wu, S. Y. Bi, X. Y. Sun, R. Zhao, J. H. Wang, H. F. Zhou, *Journal of Biomolecular Structure and Dynamics* **37(13)** (2019) 3496–3505.
[51] J. R. Flores, R. O'Kennedy, M. R. Smyth, *Analytica Chimica Acta* **212** (1988) 355–358.
[52] A. E. M. Radi, S. H. Eissa, *Eurasian Journal of Analytical Chemistry* **6(1)** (2011) 13-21.
[53] X. Chu, G. L. Shen, J. H. Jiang, T. F. Kang, B. Xiong, R. Q. Yu, *Analytica Chimica Acta* **373(1)** (1998) 29-38.
[54] M. Aslanoglu, G. Ayne, *Analytical and Bioanalytical Chemistry* **380** (2004) 658-663.
[55] C. M. A. Brett, A. N. A. Maria, O. Brett, *Electrochemistry: Principles, Methods, and Applications*, Oxford University Press, Oxford, UK, 1993, p. 444.
[56] M. Nie, Y. Wang, H. L. Li: *Polish Journal of Chemistry* **71(6)** *(*1997) 816-822.